Національна академія наук України

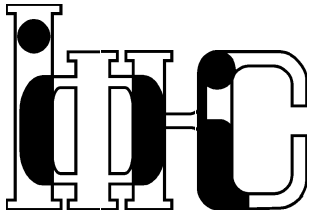

ІНСТИТУТ ФІЗИКИ КОНДЕНСОВАНИХ СИСТЕМ

ICMP–05–11E

A.P.Moina, A.G.Slivka*, V.M.Kedyulich*

Longitudinal electric field influence on the physical properties of Rochelle salt crystals

*Uzhgorod National University

ЛЬВІВ

УДК: 537.226; 537.311.33

PACS: 77.80.Bh, 77.22.Ch

Вплив поздовжнього електричного поля на фізичні властивості кристалів сегнетової солі

А.П. Моїна, О.Г. Сливка, В.М.Кедюлич

Анотація. В рамках двопідграткової моделі Міцуї з врахуванням п'єзоелектричних взаємодій вивчається вплив поздовжнього електричного поля на статичні і динамічні діелектричні, пружні, п'єзоелектричні властивості, коефіцієнт поглинання звуку в сегнетовій солі. Для польових залежностей статичної діелектричної проникності поблизу нижньої точки Кюрі отримано задовільне узгодження з експериментом, однак поблизу верхньої точки Кюрі при обчисленнях слід використовувати певні ефективні значення полів. Обговорюється можлива роль накопичення просторового заряду в екрануванні зовнішнього поля при високих температурах.

Longitudinal electric field influence on the physical properties of Rochelle salt crystals

A.P.Moina, A.G.Slivka, V.M.Kedyulich

Abstract. Influence of the longitudinal electric field on the static and dynamic dielectric, elastic, piezoelectric characteristics of Rochelle salt, as well as sound attenuation, is studied within the two-sublattice Mitsui model with taking into account the piezoelectric coupling. A satisfactory agreement with experimental data is obtained for the field effect on the static dielectric permittivity near the lower Curie temperature. At the upper Curie temperature an effective field should be used in calculations to describe the experiment. Possible role of space-charge build-up is discussed in screening of the external field at high temperatures.

Подається в physica status solidi (b)
Submitted to physica status solidi (b)

1. Introduction

A useful information about ferroelectric crystals can be given by exploring their behavior under influence of various external factors, such as high pressure or electric field. Effects produced by a static longitudinal electric field (d.c. bias applied along the axis of spontaneous polarization) in ferroelectrics undergoing second order phase transitions are well known. They include smearing out the transition, induction of polarization in the formerly paraelectric phase, increase of the permittivity maximum temperature, and decrease of its magnitude.

These effects are usually described within the Landau formalism, where the thermodynamic potential is given by the expansion

$$\Phi = \Phi_0 + \frac{\alpha}{2}P_1^2 + \frac{\beta}{4}P_1^4 - P_1E_1, \qquad (1)$$

P_1 is the crystal polarization, E_1 is the external electric field, α, β are the expansion coefficients. Anticipating subsequent consideration of Rochelle salt crystals, we suppose that the ferroelectric axis is [100].

Traditionally a linear temperature dependence $\alpha = \alpha_T(T - T_C)$ is assumed. Then the permittivity maximum magnitude $\varepsilon_{max}(E_1)$ and temperature $\Delta T_{max}(E_1)$ are expected to vary with the external field as $\sim E^{2/3}$ [1]:

$$\varepsilon_{max}^{-1} = \frac{3}{2}(4\beta)^{1/3}\varepsilon_0 E_1^{2/3} = k_1 E_1^{2/3}, \quad \Delta T_{max} = \frac{3}{4}\frac{(4\beta)^{1/3}}{\alpha_T}E_1^{2/3} = k_2 E_1^{2/3},$$

ε_0 is the dielectric permittivity of vacuum.

Rochelle salt undergoes two successive second order phase transitions, with the ferroelectric phase being the intermediate one. The permittivity maxima temperatures shift with the longitudinal field in the opposite directions. When applying the Landau theory, one can, for instance, make separate expansions near the two Curie points, with slightly different coefficients $\alpha = \alpha_{T2}(T - T_{C2})$ and $\alpha = \alpha_{T1}(T_{C1} - T)$ for the upper and low Curie temperatures, respectively. Alternatively, one can make a single expansion $\alpha = \alpha_1 + \alpha_2(T - T_0)^2$ near the temperature $T_0 = (T_{C1} + T_{C2})/2$ (a double critical point). The $\varepsilon_{max}^{-1}(E_1)$ or $\Delta T_{max}(E_1)$ dependences calculated within these two approaches are effectively the same.

When modified by the piezoelectric and elastic terms, the Landau expansion method permits to calculate the corresponding piezoelectric and elastic constants, related to them ultrasound attenuation coefficient $\varkappa$ and resonance frequencies ω_n of the crystals; their field dependences can also be explored. For Rochelle salt crystals such studies were done

e.g. in [2,3]. Overall, the Landau method predicts that the longitudinal field effect on the characteristics, diverging at the Curie points at zero field (s_{44}^E, d_{14}^E, $\varkappa$) are the same as of the static permittivity: the anomalies are smeared out, the maxima of the temperature curves are shifted.

Experimental data for the longitudinal d.c. bias influence on Rochelle salt are not very extensive and usually rather outdated. Relatively recent studies were dealt with the electric field effects on the dielectric permittivity [4–7], polarization [8], resonance frequency [9], and elastic constants [2] of the crystals. The above data were usually discussed in terms of the Landau method.

In our work, the two-sublattice Mitsui model with piezoelectric coupling [10, 11] is used to describe the above phenomena. It provides a satisfactory agreement with experiment for a number of static and dynamic dielectric, piezoelectric, and elastic characteristics of Rochelle salt in absence of external field. As we shall see later, in non-zero field the quantitative agreement is obtained at low temperatures only. Near the upper Curie point the theoretical curves for the permittivity, being qualitatively correct, overestimate the field effect and fit well to the experimental points for a much lower field than the actually applied. We believe that the electric field in crystals of Rochelle salt at high temperatures is reduced by the space charge build-up. In the external field the free charge carriers move towards the electrodes. If the electrodes are blocking for the carriers, the latters will accumulate near the electroded surfaces, forming there space charge layers. The layers, in their turn, create an internal field that reduces the total electric field in the sample.

The paper in organized as follows. In Section 2, we present the previously obtained [10,11] final expressions for the dielectric, piezoelectric, elastic, acoustic characteristics of Rochelle salt. In Section 3 we explore their dependences on the longitudinal static electric field. Conclusions are given in the last Section.

2. Model approach

Below we present the final results for the physical characteristics of Rochelle salt, previously obtained [10, 11] within the modified Mitsui model with the Hamiltonian

$$\hat{H} = U - \frac{1}{2}\sum_{qq'}\sum_{ff'=1}^{2} R_{qq'}(ff')\frac{\sigma_{qf}}{2}\frac{\sigma_{q'f'}}{2} - \Delta\sum_{q}\left(\frac{\sigma_{q1}}{2} - \frac{\sigma_{q2}}{2}\right)$$

$$- (\mu_1 E_1 - 2\psi_4\varepsilon_4)\sum_q \sum_{f=1}^{2} \frac{\sigma_{qf}}{2}. \quad (2)$$

Here

$$U = \frac{Nv}{2} c_{44}^{E0} \varepsilon_4^2 - Nv e_{14}^0 \varepsilon_4 E_1 - \frac{Nv}{2}\chi_{11}^0 E_1^2$$

is a "seed" energy of the crystal lattice which forms the asymmetric double-well potential for the pseudospins. $R_{qq'}(11) = R_{qq'}(22) = J_{qq'}$ and $R_{qq'}(12) = R_{qq'}(21) = K_{qq'}$ are constants of interaction between pseudospins belonging to the same and to different sublattices, respectively. The parameter Δ describes the asymmetry of the double well potential; μ_1 is the effective dipole moment. The last term is the internal field created by the piezoelectric coupling with the shear strain ε_4, v is a unit cell volume of the model.

Within the mean field approximation the system thermodynamic potential was obtained in the following form [10]:

$$g = \frac{U}{N} + \frac{J+K}{4}\xi^2 + \frac{J-K}{4}\sigma^2 - \frac{2\ln 2}{\beta} - \frac{1}{\beta}\ln\cosh\frac{\gamma+\delta}{2}\cosh\frac{\gamma-\delta}{2}, \quad (3)$$

where

$$\gamma = \beta\left(\frac{J+K}{2}\xi - 2\psi_4\varepsilon_4 + \mu_1 E_1\right), \quad \delta = \beta\left(\frac{J-K}{2}\sigma + \Delta\right).$$

Parameters of ferro- and antiferroelectric ordering ξ and σ are determined from the saddle point of the thermodynamic potential (3): a minimum of g with respect to ξ and a maximum with respect to σ are realized at equilibrium. J, K are Fourier-transforms (at $\mathbf{k} = 0$) of the interaction constants $J_{qq'}$ and $K_{qq'}$.

Equations for crystal polarization P_1 and lattice strain ε_4 – first derivatives of the thermodynamic potential – are [10]

$$P_1 = e_{14}^0\varepsilon_4 + \chi_{11}^{\varepsilon 0} E_1 + \frac{\mu_1}{v}\xi, \quad \varepsilon_4 = \frac{e_{14}^0}{c_{44}^{E0}} E_1 - \frac{2\psi_4}{v c_{44}^{E0}}\xi. \quad (4)$$

As it is well known, all related to the field E_1 and strain ε_4 dielectric, piezoelectric, and elastic characteristics of Rochelle salt – second derivatives of the thermodynamic potential – can be divided into two groups. Those of the first group, namely the elastic constant at constant polarization c_{44}^P and the so-called true piezoelectric constants h_{14} and g_{14} exhibit no perceptible anomaly at the Curie points at zero field. Their variation with the field E_1 is weak and will not be considered here. Those of the

other group, namely, the elastic constant at constant field c_{44}^E and the corresponding piezoelectric resonance frequencies ω_n, dielectric permittivity ε_{11}, piezoelectric coefficients d_{14} and e_{14} have strong peculiarities at the Curie points at zero field and are essentially affected by the d.c. bias.

Within the mean field approximation the dynamic dielectric permittivity, static coefficient of piezoelectric strain and static elastic constant at constant field were obtained in the form [10, 11]

$$\varepsilon_{11}(\omega) = 1 + 4\pi \times \quad (5)$$
$$\times \left\{ \frac{R(\omega)-1}{R(\omega)}\left[\chi_{11}^{\varepsilon 0} + \frac{\beta\mu_1^2}{2v}F_1(\omega)\right] + \frac{1}{R(\omega)}\left[\chi_{11}^{\sigma 0} + \frac{\beta(\mu_1')^2}{2v}F_2(\omega)\right]\right\},$$
$$d_{14} = d_{14}^0 - \frac{\mu_1'\beta\psi_4}{v c_{44}^{E0}}F_2(0), \quad c_{44}^E = c_{44}^{E0} - \frac{2\beta\psi_4^2}{v}F_1(0). \quad (6)$$

The following notations are used

$$F_1(\omega) = \frac{i\alpha\omega\lambda_1 + \varphi_3}{(i\alpha\omega)^2 + (i\alpha\omega)\varphi_1 + \varphi_2},$$
$$F_2(\omega) = \frac{i\alpha\omega\lambda_1 + \varphi_3}{(i\alpha\omega)^2 + i\alpha\omega\left[\varphi_1 - \Lambda\lambda_1\right] + \left[\varphi_2 - \Lambda\varphi_3\right]},$$
$$\varphi_2 = 1 - \frac{\beta J}{2}\lambda_1 - \beta^2\frac{K^2 - J^2}{16}(\lambda_1^2 - \lambda_2^2), \quad \varphi_1 = 2 - \frac{\beta J}{2}\lambda_1,$$
$$\varphi_3 = \lambda_1 + \beta\frac{K-J}{4}(\lambda_1^2 - \lambda_2^2), \quad \lambda_1 = 1 - \xi^2 - \sigma^2, \quad \lambda_2 = 2\xi\sigma,$$
$$\chi_{11}^{\sigma 0} = \chi_{11}^{\varepsilon 0} + e_{14}^0 d_{14}^0, \quad \mu_1' = \mu_1 - 2\psi_4 d_{14}^0, \quad d_{14}^0 = \frac{e_{14}^0}{c_{44}^{E0}},$$
$$\frac{1}{R(\omega)} = \frac{2}{kl}\tan\frac{kl}{2}, \quad k = \frac{\sqrt{\rho}\omega}{\sqrt{c_{44}^{E0}(1 - \Lambda F_1(\omega))}}, \quad \Lambda = \frac{2\beta\psi_4^2}{v c_{44}^{E0}}.$$

Here ρ is the crystal density; α is the model parameter setting the time scale of the microwave relaxation.

Expression (5) for the dynamic dielectric permittivity is obtained for a thin plate $l \times l$ of Rochelle salt crystal cut in the (100) plane. It describes an evolution of the permittivity from the static value via the piezoelectric resonances to the clamped value with the relaxational dispersion in the microwave region. The first resonance frequency and the relaxation times are [11]

$$\omega_0 = \frac{\pi}{2l}\sqrt{\frac{c_{44}^E}{\rho}}, \quad \tau_{1,2}^{-1} = \frac{1}{2\alpha}[-\varphi_1 \mp \sqrt{\varphi_1^2 - 4\varphi_2}]. \quad (7)$$

The elastic constant c_{44}^E is taken to be frequency independent, which is a good approximation in the piezoelectric resonance region.

The model developed in [11] permits also to calculate the attenuation coefficient of a transverse sound wave polarized along [010], which propagates in the 90° Z-cuts of Rochelle salt

$$\kappa(\omega) = \kappa_0 - \mathrm{Im}\,[k]\,, \tag{8}$$

$\varkappa_0$ is a frequency and temperature independent background contribution into observed attenuation (beam spreading, pulse distortion, etc).

It should be mentioned that the above expressions for dynamic characteristics were obtained [11] neglecting the contributions of the induced by electrostriction diagonal components of the lattice strain tensor ε_i $(i = 1, 2, 3)$. These contributions are zeros in the paraelectric phases, but arise in high longitudinal electric fields. To take them into account one has, however, to use an essential extension [12] of the considered here model, with a substantially increased number of fitting parameters. It is also expected that the role of electrostriction is minor as compared to that of the piezoelectricity.

3. External electric field effects

Values of the model parameters determined in [10] and providing the best fit to the calculated above characteristics are given in Table 1. Formally, no new parameter ie required to evaluate these characteristics in presence of the longitudinal electric field. However, sometimes to get a better fit to the experimental data for the dielectric permittivity taken from different papers, the value of the dipole moment μ_1 will be changed. Variation of μ_1 from sample to sample can be explained, for instance, by variation of water content, which is known to significantly affect the permittivity [4]. Interestingly, a better fit to the sound attenuation experimental data is also obtained at a value of the parameter α somewhat different from the one used to describe the microwave permittivity [7].

3.1. Static dielectric permittivity

In figs. 1,2 we show the calculated temperature dependences of dielectric permittivity ε_{11} of Rochelle salt near the upper and lower transition points at different values of external electric field. The theoretical curves are compared with independent experimental data of [4,5]. The following values of the effective dipole moments are used in calculations: $2.1 \cdot 10^{-18}$ esu cm for [4] and $2.2 \cdot 10^{-18}$ esu cm for [5].

Table 1. Model parameters for Rochelle salt [10].

J/k_B	K/k_B	Δ/k_B	ψ_4/k_B	c_{44}^{E0}	d_{14}^0	$\chi_{11}^{\sigma 0}$
	K			dyn/cm^2	esu/dyn	
797.36	1468.83	737.33	-760	$12.8 \cdot 10^{10}$	$1.9 \cdot 10^{-8}$	0.363

$v = 0.5219[1 + 0.00013(T - 190)] \cdot 10^{-21}$ cm^3,
$\mu_1 = [2.52 + 0.0066(297 - T)] \cdot 10^{-18}$ esu cm,
$\alpha = 1.7 \cdot 10^{-13}$ s.

At zero field a satisfactory quantitative description of the data is obtained in both paraelectric phases; in the ferroelectric phase the agreement is poor because of the domain contributions into the permittivity, not considered in our model. As expected, the theory yields that external field, conjugate to polarization, decreases the ε_{max} and shifts the maxima temperatures. For the upper maximum $\Delta T_{max2} > 0$, whereas for the lower one $\Delta T_{max1} < 0$. An acceptable description for the field dependences of the permittivity is obtained in the vicinity of the lower Curie temperature. In the ferroelectric phase at sufficiently high fields (above 1 kV/cm) the domain contributions into the permittivity are suppressed (a single domain state is approached), and the theory well accords with the experimental points.

However, at high temperatures a substantial deviation of the theoretical curves from experimental data both of [4] and of [5] is observed. The theory, though being qualitatively correct, strongly overestimates the field effect on the permittivity. The calculated curves coincide with the experimental points obtained in much lower fields. A question arises, what the origin of this discrepancy is.

3.2. Space-charge screening

It might be assumed that the non-linearity of the high field effects in Rochelle salt can account for the observed discrepancy between theory and experiment and should be taken into account. However, there is no reason to expect that the influence of non-linearity is so much different near the lower and upper Curie temperature. A temperature-dependent effect should be sought for. The phenomena, which role is strongly enhanced by increasing temperature (usually exponentially), are often related to the presence of free charges and conductivity in crystals. As we have already stated, we believe that the observed discrepancy between the theory and experiments in high fields near upper Curie temperature is due to screening of an external field by the space charge buildup near

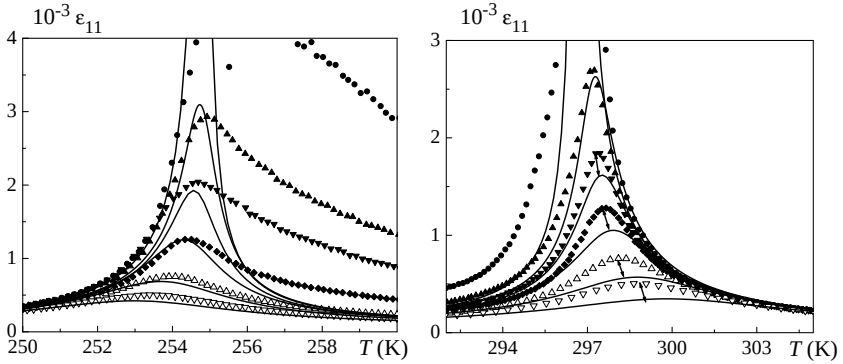

Figure 1. Temperature dependences of the dielectric permittivity of Rochelle salt at different values of external electric field E_1 (kV/cm): ● – 0, ▲ – 0.05, ▼ – 0.1, ♦ – 0.2, △ – 0.5, ▽ – 1.0. Experimental points are taken from [4]. Lines: the theory, calculated with the external field values. Arrows indicate the correspondence between the experimental points and theoretical curves.

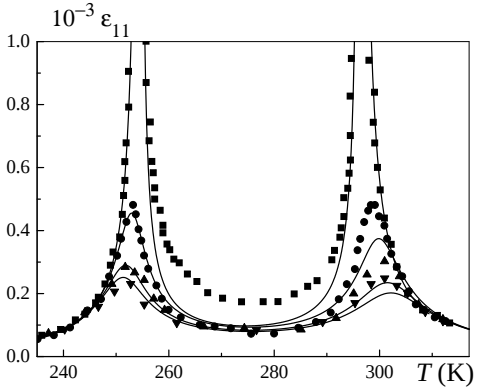

Figure 2. Same. E_1 (kV/cm): ■ – 0, ● – 0.98, ▲ – 1.97, ▼ – 2.46. Experimental points are taken from [5]. Lines: the theory, calculated with the external field values.

the electrodes.

Suppose we have a ferroelectric crystal of the thickness L along the axis of spontaneous polarization x, with positive and negative free charges also present. When an external voltage V_0 along the x axis is applied, the crystal gets polarized, and the free charges start to move towards the electrodes. If the electrodes are blocking, the free charges will pile up at them, forming two space-charge layers near the electroded crystal surfaces. Direction of the electric field created by these layers is opposite to the direction of the external field; it screens out the external field in the bulk of the crystal. As we shall show later, for Rochelle salt the screening of the external field by the space-charge buildup at the electrodes is only partial.

The charge carrier concentration is expected to decrease exponentially with decreasing temperature. The field created by the space charge layers will decrease too; that is why the screening is practically not observed near the lower Curie temperature.

The discussed above effect of the space charge build-up under application of d.c. bias, resulting in partial reduction of the externally applied field in the bulk of the samples, has been actually detected experimentally by Triebwasser in $BaTiO_3$ [13]. The $BaTiO_3$ is a n-type semiconductor with high donor carrier concentration but low carrier mobility. The time constants associated with the space-charge buildup were found to be of the order of one or two minutes.

3.3. Effective field

Partial screening of the external field is well shown by the following calculations. We evaluate the permittivity (5) near the upper Curie temperature using a certain effective field E_{eff} instead of the actually applied in the experiment E_{ext}. As seen in fig. 3, we obtain a nearly perfect fit to the experimental data, especially at high fields, when the domain effects are suppressed.

The correspondence between the external fields and effective fields used to fit to the experimental data is given in the table below and in fig. 4. As one can see the dependence $E_{eff}(E_{ext})$ is approximately linear, with the ratio E_{eff}/E_{ext} of about $0.55 \div 0.75$ above 0.5 kV/cm both for the experimental points of [4] and of [5]. Below 0.5 kV/cm the obtained difference between E_{eff} and E_{ext} is less significant.

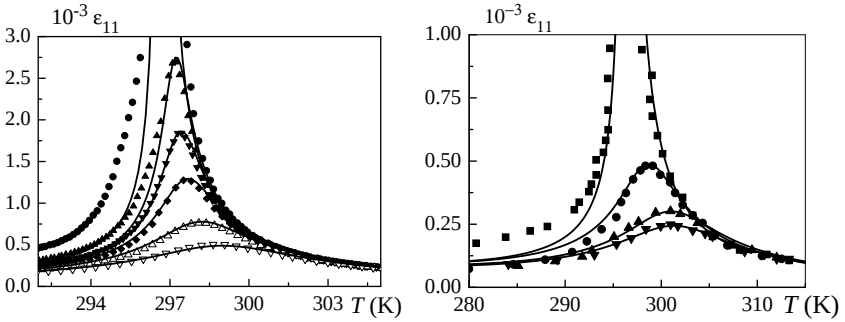

Figure 3. Dielectric permittivity near the upper Curie temperature at different values of electric field. Experimental points are taken from [4] (left) and [5] (right). Values of external fields are the same as in figs. 1 and 2. Lines: the theory calculated at some effective fields (see text).

	using the data of [4]					
E_{ext} (kV/cm)	0.05	0.1	0.2	0.3	0.5	0.75
E_{eff} (kV/cm)	0.045	0.081	0.14	0.2	0.3	0.42
E_{eff}/E_{ext}	0.9	0.81	0.7	0.67	0.6	0.56

	using the data of [5]		
E_{ext} (kV/cm)	1	1.97	2.46
E_{eff} (kV/cm)	0.6	1.36	1.86
E_{eff}/E_{ext}	0.6	0.69	0.76

In subsequent calculations we shall use the values of the effective fields from the table above and $E_{eff} \sim 0.6E_{ext}$ at $E_{ext} > 2$ kVcm near the upper transition point. Near the lower transition point we take $E_{eff} = E_{ext}$. A linear interpolation between these two values in assumed for the ferroelectric phase.

3.4. Polarization and other static properties

Figure 5 illustrates the field effect on the temperature dependences of the polarization P_1 and lattice strain ε_4 of Rochelle salt. The experimental points are for zero field. The expected behavior in non-zero fields (induced polarization and ε_4 in the formerly paraelectric phases) is obtained. The field influence enhances on lowering temperature, as the effective field approaches the external one. No quantitative comparison with experiment at non-zero field is attempted, for the following reasons.

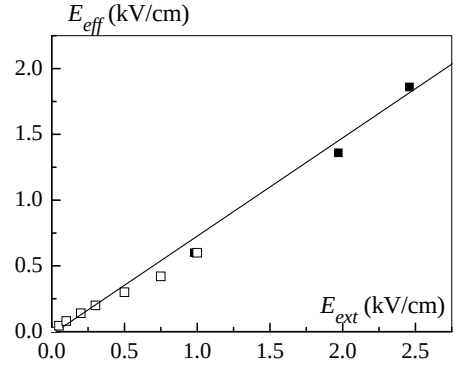

Figure 4. Effective field vs external field near the upper Curie temperature, as determined by fitting to the data of [4] (□) and [5] (■).

First, the deviation of the theory for spontaneous polarization from experiment (at zero field) is larger than the predicted field effects. Then, the expression (4) takes into account the contribution of the ordering units only. Essential, especially at high temperatures and fields, is the contribution of the space-charge polarization. A quantitative comparison to experiment at $E_1 \neq 0$ without taking it into account is pointless.

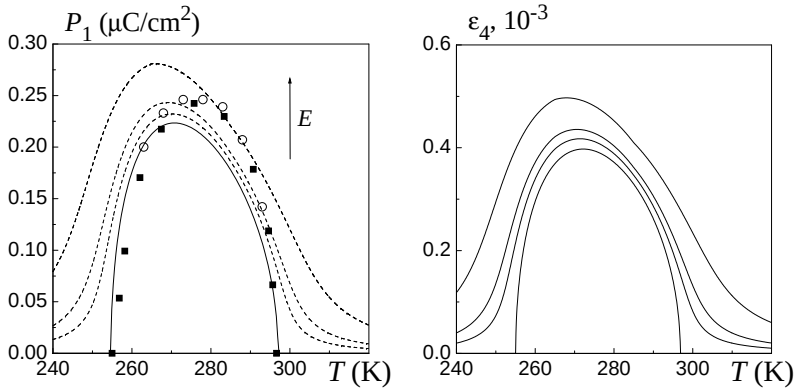

Figure 5. Temperature dependences of polarization P_1 and strain ε_4 at different values of external electric field E_{ext} (kV/cm): 0, 1, 2, 6. Choice of the effective field E_{eff} – see text. Experimental points taken from ○– [14]; ■ – [15] correspond to the zero field case.

In figure 6 we show the calculated temperature curves of the elastic

constant c_{44}^E and coefficient of piezoelectric strain d_{14} at different values of d.c. bias. As one can see, their field dependences are qualitatively similar to those of the static dielectric permittivity ε_{11}. It should be mentioned, however, that the shifts of the maxima (minima) temperatures of these characteristics with the field are slightly different, because of the dipole moment μ_1 taken as a linear function of temperature, and since $\varepsilon_{11} \sim (\mu_1 - 2d_{14}^0\psi_4)^2$, $d_{14} \sim \mu_1 - 2d_{14}^0\psi_4$, and c_{44}^E depends on μ_1 only implicitly via ξ. No satisfactory experimental data for non-zero fields to be compared with the theory was available. The data of [2] for the $c_{44}^E(E_{ext})$ cannot be used because of their strong dependence on the field sign.

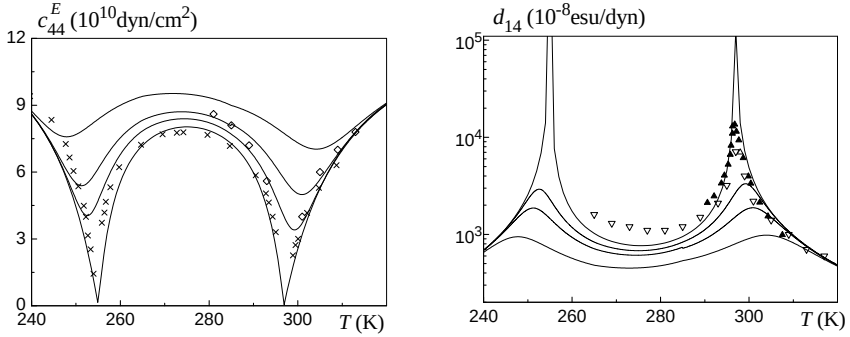

Figure 6. Temperature dependences of the elastic constant c_{44}^E and coefficient of piezoelectric strain d_{14} at different values of external electric field E_{ext} (kV/cm): 0, 1, 2, 6. Choice of the effective field E_{eff} – see text. Experimental points taken from $\times$ – [2], $\Diamond$ – [16], $\bigtriangledown$ – [17], $\blacktriangle$ – [18] correspond to the zero field case.

3.5. Dynamic permittivity

As seen in fig. 6, the elastic constant c_{44}^E is increased by the field at any temperature. It means that the resonance frequencies are also increased; this accords with the experimental data [9, 19]. The increase of the first resonance frequency (and of the overtones) determines the field influence on the dielectric dynamic permittivity in the piezoelectric resonance region. Figure 7 illustrates the field effects on the permittivity of a 1×1 cm^2 cut of a Rochelle salt crystal near the upper Curie point at different frequencies within this region.

As can be seen, application of the field is, in a sense, similar to lowering frequency. When at zero field the measuring frequency is just above

the first resonance peak (first row of Fig. 7), a sufficiently high field can make it lower than the first resonance peak. We obtain a picture characteristic of a static permittivity under the d.c. bias. Increasing frequency at zero field (the second row) multiplies the number of resonance peaks. The electric field decreases the number of resonance peaks back and shift them apart. The peaks remain as sharp as in zero field, no smearing is observed.

At the upper part of the resonance region (the third row) at zero field the permittivity curve has both the central peak structure at the transition point and numerous side resonance peaks. In the field the central peak is smeared out, its magnitude is decreased. The field also shifts the resonances closer to the central peak, as would happen on lowering frequency. The resonance peaks stay sharp.

Interesting field effects are observed for the dielectric permittivity in the microwave region. At low frequencies of this region (below 5 GHz) the permittivity has finite peaks at the transition points. The field, as in the static case, smears out the peaks and shift the rounded maxima towards the corresponding formerly paraelectric phases (see fig. 8). At higher frequencies and zero field, the permittivity has shallow minima at the transition points and a pair of rounded maxima at both sides of each minimum [7]. Application of d.c. bias smears out the minima, and each pair of maxima tends to coalesce. At sufficiently high fields the maxima finally merge, and the minima disappear. This behavior is illustrated in fig. 8, and it accords qualitatively with the experimental results of [7]. Quantitative agreement with experiment is fair and approximately the same at all fields.

Field influence on the inverse relaxation times is shown in fig. 9. The relaxation time τ_1, exhibiting critical slowing down at the Curie points and zero field (but remaining finite due to piezoelectric clamping effect), varies with the field in the same manner as the dielectric permittivity of a clamped crystal (see fig. 8 for $\nu = 2.5$ GHz). The second relaxation time, whose contribution to the permittivity is minor, is increased by the field.

Decrease of the relaxation time τ_1 with the field means an increase of the microwave dispersion frequency, as follows from the relation $\omega\tau = 1$. The shift of the dispersion frequency with the bias is well seen in the fig. 10, where the frequency dependences of real and imaginary parts of the dynamic dielectric permittivity in the microwave region are presented.

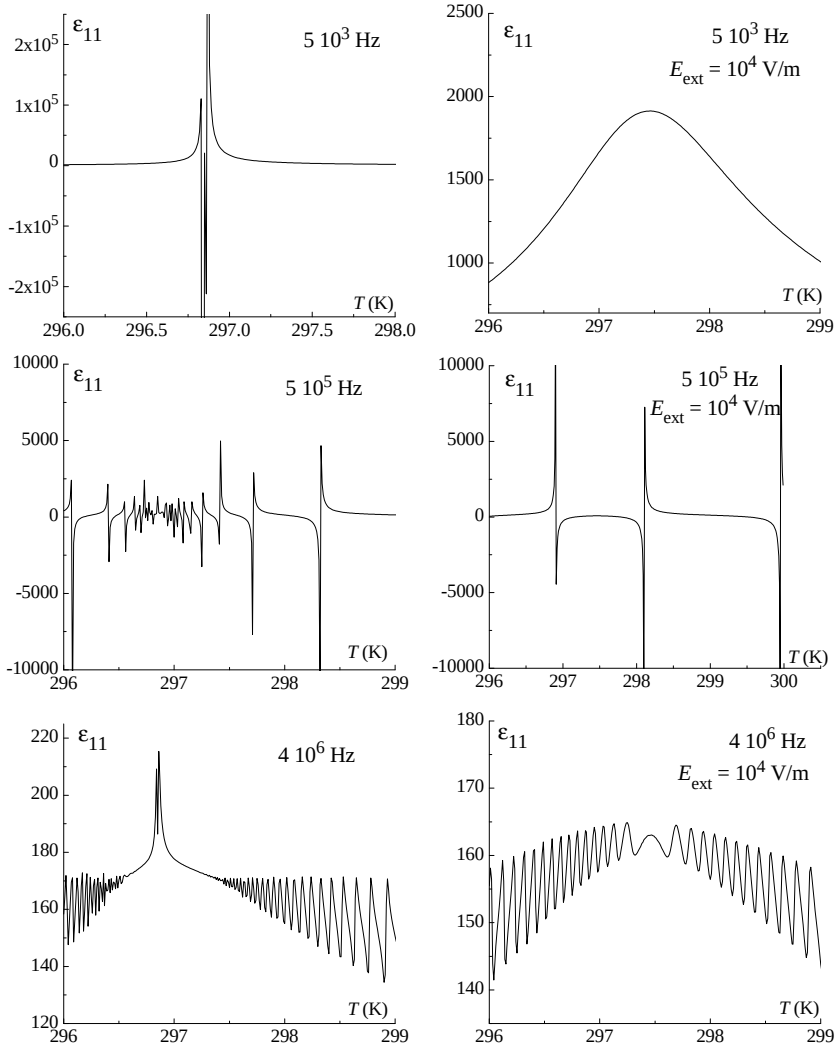

Figure 7. Dynamic dielectric permittivity in piezoelectric resonance region at different frequencies and fields E_{ext}: 0 (left), 10^4 V/m (right). E_{eff} is used in calculations.

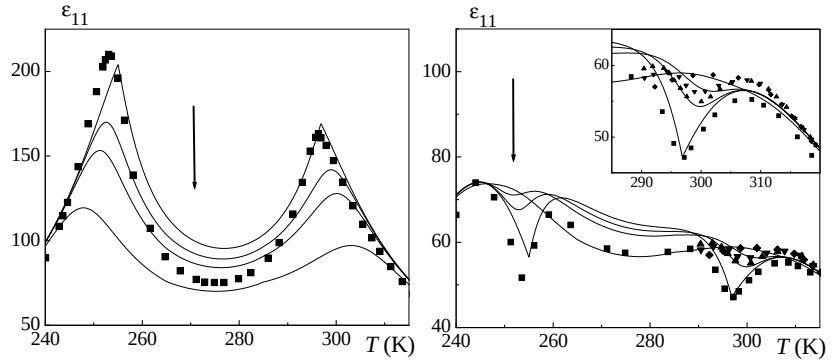

Figure 8. Dynamic dielectric permittivity in the microwave region at $\nu =$ 2.5 GHz (left) and 8.25 GHz (right). Choice of the effective field E_{eff} – see text. Experimental points [7] are for E_{ext} (kV/cm): ■ – 0, ▲ – 1, ▼ – 2, ♦ - 6.

3.6. Sound attenuation

Closely related to the discussed relaxation times is the ultrasound attenuation coefficient κ for the transverse wave propagating in 90° Z-cuts of Rochelle salt. It exhibits a critical behavior at the transition points, and the d.c. bias is expected to smear out this criticality. The field dependences of this attenuation in Rochelle salt were calculated in [3] within the Landau approach. In fig. 8 we depict the theoretical curves obtained within the modified Mitsui model with $\kappa_0 = 0.5$ cm^{-1} and $\alpha = 2.3 \cdot 10^{-13}$ s, which qualitatively agree with the those obtained in [3]. As can bee seen, the presented field dependences of attenuation are analogous to those of static permittivity or piezomodule d_{14}.

The external field weakens the frequency dependence of sound attenuation at low frequencies (see fig. 12, left). In the microwave region an existence of a cut-off frequency for sound propagation is expected [11], which frequency position correlates with the start of a fast increase in the imaginary part of the dielectric permittivity. The longitudinal field strongly increases the cut-off frequency (see fig. 12, right). Similarly to the previously discussed shift of the microwave relaxation frequency, this is also due to the decrease of the relaxation time τ_1 with the field.

4. Concluding remarks

In the present paper the influence of longitudinal electric field on the static and dynamic dielectric, elastic, piezoelectric characteristics of Rochelle

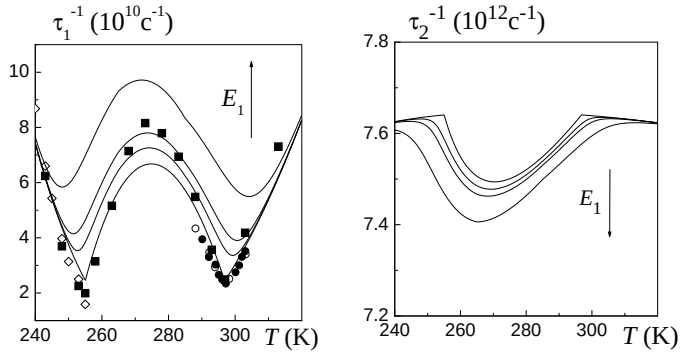

Figure 9. Temperature dependences of inverse relaxation times at different values of external field E_{ext} (kV/cm): 0, 1, 2, 6. Choice of the effective field E_{eff} – see text. Experimental points for zero field are taken from • – [20], ○– [21], ■ – [7], ◊ – [22].

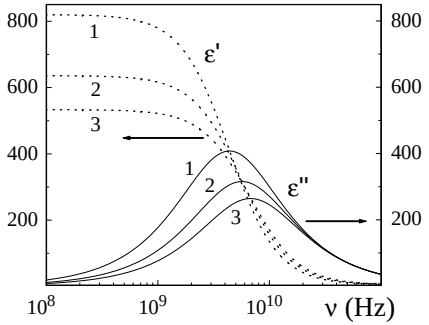

Figure 10. Frequency dependence of real and imaginary parts of dynamic dielectric permittivity in the microwave region at 298 K and different values of external electric field E_{ext} (kV/cm): 1 – 0, 2 – 1, 3 – 2.

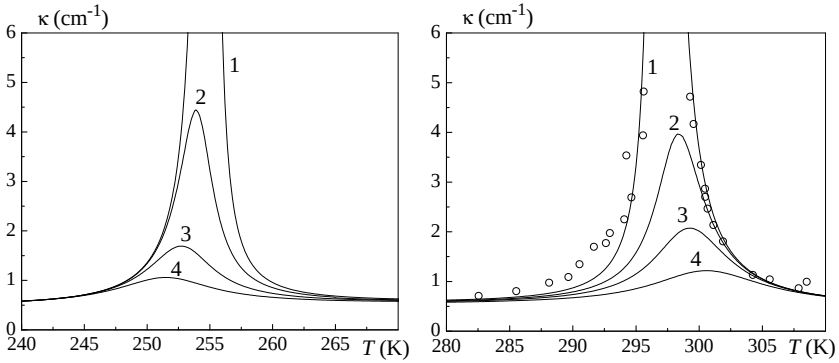

Figure 11. Temperature dependence of sound attenuation in Rochelle salt near the lower and upper Curie temperatures at $\nu = 10^7$ Hz and different values of external electric field E_{ext} (kV/cm): 1 – 0, 2 – 0.5, 3 – 1, 4 – 2. Experimental points taken from [16] correspond to the zero field case. Choice of E_{eff} used in calculations – see text.

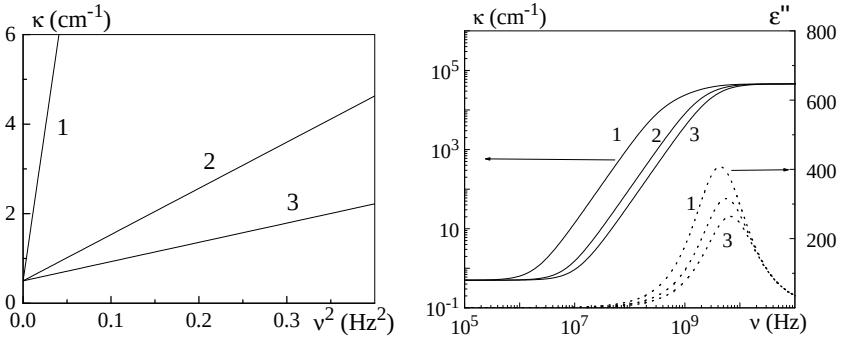

Figure 12. Frequency dependence of attenuation at 298 K and different values of external electric field E_{ext} (kV/cm): 1 – 0, 2 – 1, 3 – 2. Dashed line: imaginary part of dielectric permittivity. Choice of E_{eff} used in calculations – see text.

salt, as well as sound attenuation, is studied within the two-sublattice Mitsui model with taking into account the piezoelectric coupling. The calculation results are compared with available recent experimental data.

A satisfactory agreement is obtained for the field effect on the static dielectric permittivity near the lower Curie temperature. However, at the upper Curie temperature an effective field of about $0.6E_{ext}$ should be used in calculations to fit to the experimental points. The experimental field effect on the microwave permittivity is also fairly well described by the presented theory with the effective fields used in calculations.

Theory predictions for the field influence on the elastic constant c_{44}^E, piezomodule d_{14}, attenuation coefficient κ for 90° Z-cut of Rochelle salt, relaxation times τ_i, as well as the dynamic dielectric permittivity in the piezoelectric resonance region are presented. The expected field dependences of c_{44}^E, d_{14}, κ, τ_1 are similar to those of static permittivity. On the contrast, the temperature behavior of the permittivity in the resonance region can be qualitatively changed by the external field; this is due to the increase of the resonance frequencies with the field.

In the microwave region an existence of a cut-off frequency for sound propagation in 90° Z-cut is expected [11]. The longitudinal field has been shown to strongly increase the cut-off frequency, as well as the microwave dielectric relaxation frequency. These effects are due to the decrease of the relaxation time τ_1 with the field.

It is argued that the origin of external field screening at high temperatures is the space-charge build-up at blocking electrodes. A presumed exponential decrease of charge carrier concentration with decreasing temperature explains why screening is not observed near the lower Curie temperature. No attempt to explicitly describe space-charge buildup has been undertaken in the present paper. This problem will be the subject of a separate publication. Such calculations will permit to describe the field dependences of polarization, where the contribution of the space-charge polarization must be taken into account.

Acknowledgement

We acknowledge support of Fundamental Research State Fund of Ukraine, project No 02.07/00310. We also greatly appreciate useful discussions of the presented results with Prof. I.V. Stasyuk, Prof. R.R. Levitskii, and Prof. M.O.Romanyuk.

References

1. M. Lines, A. Glass. Principles and application of ferroelectrics and related materials, (Clarendon Press, Oxford, 1977).
2. O.Yu. Serdobolskaya, Sol. Stat. Phys. **38**, 1529 (1996).
3. S.Ya. Geguzina, B.L. Timan, Solid Stat. Phys. **9**, 2167 (1967) (in Russian).
4. A.G. Slivka, V.M. Kedyulich, R.R. Levitskii, A.P. Moina, M.O. Romanyuk, A.M. Guivan, Condens. Matter Phys., **8**, **No 3(43)**, 638 (2005).
5. K. Gesi, K. Ozawa, J. Phys. Soc. Japan **48**, 2003 (1992).
6. I.H. Ismailzade, O.A. Samedov, A.I. Alekberov, phys. stat. sol.(a) **94**, K17 (1986).
7. F. Sandy and R.V. Jones, Phys. Rev. **168**, 481 (1968).
8. V.V. Gladkii, E.I. Marchenko, A.S. Sonin, Solid State Phys. **10**, 478-481 (1968) (in Russian).
9. D.J. Jefferies, Physics Letters **90A, No 6**, 316 (1982).
10. R.R. Levitskii, I.R. Zachek, T.M. Verkholyak, A.P. Moina, Phys. Rev. B. **67**, 174112 (2003).
11. A.P. Moina, R.R. Levitskii, I.R. Zachek, Phys. Rev. B **71**, 134108 (2005).
12. R.R. Levitskii, I.R. Zachek, A.P. Moina, to appear in Condens. Matter Phys. **8**, **No 4(44)** (2005).
13. S. Triebwasser, Phys. Rev., 1960 **118**, 100.
14. W.G. Cady, Piezoelectricity; an introduction to the theory and application of electromechanical phenomena in crystals. (New York, London. McGraw Hill Book Company, Inc., 1946.)
15. J Hablützel., Helv. Phys. Acta **12**, 489 (1939).
16. W.J. Price, Phys. Rev. **75**, 946 (1949).
17. L. Gutin. Zh. Eksp. Teor. Fiz. (Sov. Phys. — JETP) **15**, 199 (1945).
18. H. Beige, A.Kühnel, Phys. Stat. Sol.(a) **84**, 433 (1984).
19. H. Mueller, Phys. Rev, 1940 **58**, 565.
20. H.E. Müser, J.Pottharst, Phys. Stat. Sol. **109**, (1967).
21. Kolodziej H. In Dielectric and Related Molecular Processes. vol.2, London WIVOBN, The Chemical Society Burlington House, 1975, p.249–287.
22. A.A. Volkov, G.V.Kozlov, S.P. Lebedev. Zh. Eksp. Teor. Fiz. **79**, 1430 (1980).

Препринти Інституту фізики конденсованих систем НАН України розповсюджуються серед наукових та інформаційних установ. Вони також доступні по електронній комп'ютерній мережі на WWW-сервері інституту за адресою http://www.icmp.lviv.ua/

The preprints of the Institute for Condensed Matter Physics of the National Academy of Sciences of Ukraine are distributed to scientific and informational institutions. They also are available by computer network from Institute's WWW server (http://www.icmp.lviv.ua/)

Алла Пилипівна Моїна
Олександр Георгійович Сливка
Віктор Михайлович Кедюлич

Вплив поздовжнього електричного поля на фізичні властивості кристалів сегнетової солі

Роботу отримано 22 листопада 2005 р.

Затверджено до друку Вченою радою ІФКС НАН України

Рекомендовано до друку семінаром відділу теорії модельних спінових систем

Виготовлено при ІФКС НАН України